The Astrophysical Journal, 669: L53–L56, 2007 November 1

FREE MAGNETIC ENERGY IN SOLAR ACTIVE REGIONS ABOVE THE MINIMUM-ENERGY RELAXED STATE

S. Régnier and E. R. Priest
School of Mathematics, University of St. Andrews, St. Andrews, Fife KY16 9SS, UK
Received 2007 August 3; accepted 2007 September 7; published 2007 October 5

ABSTRACT

To understand the physics of solar flares, including the local reorganization of the magnetic field and the acceleration of energetic particles, we have first to estimate the free magnetic energy available for such phenomena, which can be converted into kinetic and thermal energy. The free magnetic energy is the excess energy of a magnetic configuration compared to the minimum-energy state, which is a linear force-free field if the magnetic helicity of the configuration is conserved. We investigate the values of the free magnetic energy estimated from either the excess energy in extrapolated fields or the magnetic virial theorem. For four different active regions, we have reconstructed the nonlinear force-free field and the linear force-free field corresponding to the minimum-energy state. The free magnetic energies are then computed. From the energy budget and the observed magnetic activity in the active region, we conclude that the free energy above the minimum-energy state gives a better estimate and more insights into the flare process than the free energy above the potential field state.

Subject headings: Sun: activity — Sun: corona — Sun: coronal mass ejections (CMEs) — Sun: flares — Sun: magnetic fields

1. INTRODUCTION

Due to the low value of the plasma β (the ratio of gas pressure to magnetic pressure), the solar corona is magnetically dominated. To describe the equilibrium structure of the coronal magnetic field when gravity is negligible, the force-free assumption is then appropriate:

$$\nabla \wedge \boldsymbol{B} = \alpha \boldsymbol{B}, \tag{1}$$

where $\alpha = 0$ gives the potential (or current-free) field, $\alpha =$ constant gives the linear force-free (LFF) field, and α being a function of space gives the nonlinear force-free (NLFF) field. The properties of force-free fields have been well described (e.g., Woltjer 1958; Molodenskii 1969; Aly 1984; Berger 1985). Woltjer (1958) with general astrophysical configurations in mind derived two important theorems: (1) in the ideal MHD limit the magnetic helicity is invariant during the evolution of any closed flux systems; (2) the minimum-energy state is the linear force-free field conserving the magnetic helicity (see also Aly 1984; Berger 1985). Taylor (1986) applied this to laboratory experiments and hypothesized that in a weak but finite resistive regime the total magnetic helicity of the flux system is invariant during the relaxation process to a minimum-energy state. According to Woltjer (1958) the relaxed state is then a linear force-free field. Therefore the free magnetic energy that can be released during a relaxation process is the excess energy of the magnetic configuration above the linear force-free field with the same magnetic helicity.

Heyvaerts & Priest (1984) were the first to suggest the importance of magnetic helicity and Taylor relaxation in the solar corona. They extended the Woltjer-Taylor theory for an isolated structure bounded by magnetic surfaces to that of a coronal field in which the field lines enter or leave the volume (through the photosphere): thus the magnetic helicity is allowed to enter or leave the corona as the photospheric field changes in time. They also suggested that the coronal field evolves locally through a set of linear force-free fields with the field continually relaxing and the footpoint connections continually changing by small-scale turbulent reconnections, which heat the corona. Moreover they suggested that, if the magnetic helicity becomes too large, an eruption takes place in order to expel the excess magnetic helicity. The coronal heating mechanism by magnetic turbulent relaxation was later developed into a self-consistent theory (Heyvaerts & Priest 1992). Based on a statistical analysis of vector magnetograms, Nandy et al. (2003) have shown that the relaxation process of flare-productive active regions is similar to Taylor's theory. Nevertheless, Régnier & Canfield (2006) have shown that the magnetic helicity can evolve significantly on a short timescale (about 15 minutes) and that the evolution of the coronal magnetic field is often well described by a series of nonlinear force-free equilibria. The modeled evolution of global coronal fields by successive nonlinear force-free equilibria was also investigated by Mackay & van Ballegooijen (2006a, 2006b).

To better understand the physics of flares, we need to estimate the amount of magnetic energy available in a magnetic configuration for conversion into kinetic energy and/or thermal energy in a solar flare. There is no free magnetic energy in a potential field configuration: this is a minimum-energy state for a given normal magnetic field at the photosphere, and the magnetic energy depends only on the distribution and amount of flux through the photosphere. The linear and nonlinear configurations, however, do have free energy due to the presence of currents. As shown in Régnier & Priest (2007) the energy storage in active regions can be (1) in the corona due to the existence of large-scale twisted flux bundles, or (2) near the base of the corona associated with the existence of a complex topology. The free energy can be estimated from photospheric or chromospheric magnetic fields based on the magnetic virial theorem (Molodenskii 1969; Aly 1984), or from reconstructed 3D coronal fields (often assuming a force-free equilibrium). Using nonlinear force-free fields, the magnetic energy budget has been estimated before and after a flare (Bleybel et al. 2002; Régnier & Canfield 2006): as expected the authors found that the magnetic energy usually decreases during the flare. Nevertheless, this energy strongly depends on the strength of the flare, on the processes of energy injection (e.g., flux emergence, flux cancellation, sunspot rotation), and on the time span between the reconstructed fields. Bleybel et al. (2002) have suggested that Taylor's theory does not apply to flares and CMEs.

The same conclusion has been reached previously by numerical simulations (see, e.g., Amari & Luciani 2000). This can be understood if (1) the helicity is not conserved during a flare or a CME in the finite domain of computation due to the injection of helicity through the photosphere or into the CMEs, and (2) the eruption phenomenon is often localized in the active region and so does not affect or modify strongly the nonpotentiality of the field outside the flare surroundings. Note that the energy flux (or Poynting flux) can be derived from successive magnetic field measurements when the plasma flows are known (see, e.g., Kusano et al. 2002). The Poynting flux gives an estimate of the injected energy through the photospheric surface due to transverse motions and/or flux emergence.

In this Letter, we compute the free magnetic energy for different active regions assuming a nonlinear force-free equilibrium with a reference field being either the potential field or the linear force-free field. We also compute the magnetic energies from the magnetic virial theorem. We are assuming that at a given time and with the same boundary conditions the minimum-energy state is given (Woltjer's theorem) by the linear force-free field with the same magnetic helicity as the nonlinear force-free field. We are not here investigating the validity of the Taylor-Heyvaerts theory in solar active regions.

2. SELECTED ACTIVE REGIONS

In order to compare the different measurements of free magnetic energy, we have selected four different active regions with different types of activity (confined flares, flares associated with a CME, or filament eruptions) and at a different stage of their evolution (before or after a flare):

AR 8151.—Observed on 1998 February 11 at 17:36 UT, this is an old decaying active region (decreasing magnetic flux and magnetic polarities diffusing away). A filament eruption associated with an aborted CME was reported on February 12, but no flare was observed. The vector magnetic field was recorded by the Mees IVM (Mickey et al. 1996; LaBonte et al. 1999). The high values of the current density imply strongly sheared and twisted flux bundles (see Régnier et al. 2002; Régnier & Amari 2004). Due to the existence of highly twisted flux tubes (with more than 1 turn) and the stability of the reconstructed filament and sigmoid (with less than 1 turn), the authors concluded that the eruptive phenomenon was most likely to be due to the development of a kink instability in the highly twisted flux bundles.

AR 8210.—Observed on 1998 May 1 from 17:00 to 21:30 UT, this is a newly emerged active region with a complex topology as described in Régnier & Canfield (2006). An M1.2 flare was recorded on 1998 May 1 at 22:30 UT. The selected vector magnetogram (Mees IVM) at 19:40 UT was observed during a "quiet" period between two C-class flares. In Régnier & Canfield (2006) the authors described the magnetic reconnection processes occurring during this time period and leading to a local reorganization of the magnetic field. The reconnection processes are related to the slow clockwise rotation of the main sunspot or a fast moving, newly emerged polarity. Following the time evolution during 4 hours, the authors showed that the free magnetic energy decreases during the flare over a period of about 15 minutes, and the total magnetic energy is slightly increased during this time period.

AR 9077.—This corresponds to the famous Bastille Day flare in 2000 (e.g., Liu & Zhang 2001; Yan et al. 2001; Fletcher & Hudson 2001). The vector magnetogram was recorded at 16:33 UT after the X5.7 flare which occurred at 10:30 UT. The active region was still in the magnetic reorganization phase after the flare and "post"-flare loops were observed in 195 Å *TRACE* EUV images. The flare was also associated with a CME.

AR 10486.—This active region is responsible for the main eruptions observed during the Halloween events (2003 October 26 to November 4). The Mees IVM vector magnetogram was recorded on 2003 October 27 at 18:36 UT before the X17.2 flare which occurred at 11:10 UT on October 28. The flaring activity of this active region and the associated CMEs have been extensively studied. For instance, Metcalf et al. (2005) have shown that the large magnetic energy budget ($\sim 3 \times 10^{33}$ erg) on October 29 is enough to power the extreme activity of this active region.

For these particular active regions, the reduction of the full Stokes vector to derive the magnetic field has already been detailed in several articles (e.g., Régnier et al. 2002; Régnier & Canfield 2006); the 180° ambiguity in the transverse component was solved by using the algorithm developed in Canfield et al. (1993).

3. MAGNETIC FIELDS

From the observed vector magnetic field as described in § 2, we extrapolate to obtain three types of coronal magnetic field, each of which has the vertical component of the magnetic field imposed at the photosphere:

1. *Potential field*.—There is no current flowing in the magnetic configuration; this is the minimum-energy state that the magnetic field can reach when the magnetic helicity is not conserved.
2. *Linear force-free field*.—We compute the linear force-free field whose α-parameter is chosen so that the total magnetic helicity is the same as the nonlinear force-free field; in other words, this gives the minimum-energy state that conserves the magnetic helicity. The LFF field is computed in a finite domain which avoids the problems of an unbounded domain, namely the energy being infinite and the field possessing unphysical reversals. This is a reasonable approximation to a more realistic model in which a linear force-free active region is immersed in a larger scale magnetohydrostatic or MHD region.
3. *Nonlinear force-free field*.—We use the vector potential Grad-Rubin-like method (Grad & Rubin 1958; Amari et al. 1997, 1999). The bottom boundary conditions also require the knowledge of α in one polarity derived from the transverse field components: $\alpha = (1/B_z)(\partial B_y/\partial x - \partial B_x/\partial y)$. The Grad-Rubin numerical scheme solves the NLFF equations by first transporting α from one polarity into the domain and then by updating the 3D field to a new NLFF equilibrium. We use closed boundary conditions on the sides and the top of the domain.

In order to have energy values which can be compared, we have imposed the same closed conditions on the side and top boundaries for each model. To satisfy these conditions, we surround the vector magnetic field observed by the Mees IVM by weak-field measurements provided by *SOHO* MDI line-of-sight observations. The active region fields are then confined by a surrounding potential field and the magnetic field decreases from the center of the active region (compatible with the field vanishing at infinity). The magnetic flux is balanced in order to ensure that the closed boundary conditions on the sides and the top of the domain are consistent with $\nabla \cdot \boldsymbol{B} = 0$.

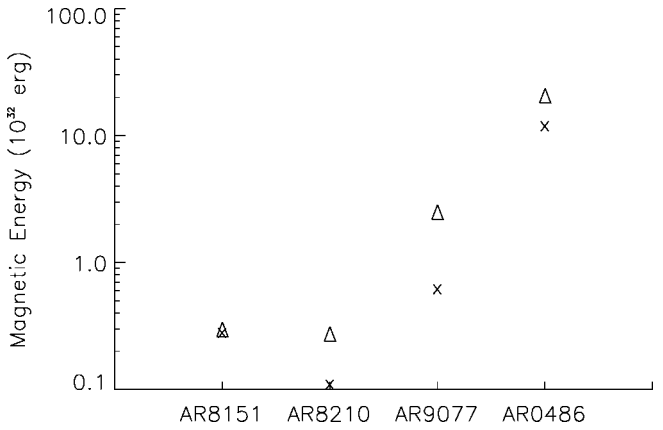

FIG. 1.—Magnetic energy above potential for both the NLFF field (*triangles*) and the LFF field (*crosses*) of the four selected active regions (units of 10^{32} erg). The free magnetic energies $\Delta E_{\rm LFF}^{\rm NLFF}$ are given by the differences between the triangles and crosses.

4. FREE MAGNETIC ENERGY

From the 3D coronal magnetic configurations, we can derive the magnetic energy for the different active regions and different models:

$$E_m = \int_\Omega \frac{B^2}{8\pi}\, d\Omega \tag{2}$$

in a volume Ω. The free magnetic energy is derived from the nonlinear force-free (NLFF) field using either the potential or linear force-free (LFF) field as reference field:

$$\Delta E_{\rm pot}^{\rm NLFF} = E_m^{\rm NLFF} - E_m^{\rm pot}, \quad \Delta E_{\rm LFF}^{\rm NLFF} = E_m^{\rm NLFF} - E_m^{\rm LFF}. \tag{3}$$

The LFF field used here has the same relative magnetic helicity as the NLFF field satisfying Woltjer's theorem. That implies that the NLFF field has to be computed first, and then the LFF field is determined by an iterative scheme to find the α-value matching the helicity of the NLFF field. The relative magnetic helicity is computed from the Berger & Field (1984) equation (see, e.g., Régnier et al. 2005):

$$\Delta H_m = \int_\Omega (\boldsymbol{A} - \boldsymbol{A}_{\rm pot}) \cdot (\boldsymbol{B} + \boldsymbol{B}_{\rm pot})\, d\Omega, \tag{4}$$

where $\boldsymbol{B}$ and $\boldsymbol{A}$ ($\boldsymbol{B}_{\rm pot}$ and $\boldsymbol{A}_{\rm pot}$) are the NLFF (potential) magnetic field and its associated vector potential computed in the volume Ω. The relative magnetic helicity given by equation (4) satisfies the closed boundary conditions used by the Grad-Rubin reconstruction method.

For the sake of comparison, we also compute the free magnetic energy derived from the magnetic virial theorem assuming a force-free field (e.g., Aly 1989; Klimchuk et al. 1992; Metcalf et al. 1995, 2005; Wheatland & Metcalf 2006). Considering that the magnetic field can be decomposed into a potential part and a nonpotential one, $\boldsymbol{B} = \boldsymbol{B}_{\rm pot} + \boldsymbol{b}$, then following Aly (1989) the free magnetic energy (above potential) is

$$\Delta E_m^{\rm vir} = \frac{1}{4\pi} \int_\Sigma (x b_x + y b_y) B_z\, dx\, dy \tag{5}$$

in the half-space above the surface Σ. The free magnetic energy from the virial theorem only requires the magnetic field distribution on the bottom boundary as we use closed boundary conditions on the other boundaries. We compute equation (5) from either the observed vector magnetic field (not necessarily force-free) or the reconstructed NLFF field on the photosphere. It is important to note that the energy values derived from the magnetic virial theorem are strongly influenced by the spatial resolution as mentioned in Klimchuk et al. (1992).

In Figure 1 we plot the free energy values in the reconstructed magnetic configurations using the potential field as reference field for the NLFF fields (*triangles*) and LFF fields (*crosses*). The difference between the two values is the minimum free energy $\Delta E_{\rm LFF}^{\rm NLFF}$ according to Woltjer's theorem. Figure 1 clearly shows that the free magnetic energy can vary by at least 2 orders of magnitude: the energy is strongly influenced by the total magnetic flux and the distribution of the polarities. By comparing the amount of free energy $\Delta E_{\rm pot}^{\rm NLFF}$ and the observed eruptive phenomena, we can conclude that $\Delta E_{\rm LFF}^{\rm NLFF}$ gives a better estimate of the free energy. For instance, $\Delta E_{\rm pot}^{\rm NLFF}$ is similar for AR 8151 and AR 8210 but $\Delta E_{\rm LFF}^{\rm NLFF}$ is nearly 3 times larger for AR 8210. And the related eruptive phenomena are very different: a slow filament eruption without a flare for AR 8151 and a C-class flare for AR 8210. For AR 9077, $\Delta E_{\rm LFF}^{\rm NLFF}$ is still enough to trigger an X-class flare but certainly not the X5.7 flare observed prior to the time considered here. For AR 10486, $\Delta E_{\rm LFF}^{\rm NLFF}$ is significantly reduced compared to $\Delta E_{\rm pot}^{\rm NLFF}$ but still enough to trigger powerful flares, which explains the high level of activity in this active region (Metcalf et al. 2005).

In Table 1 we summarize the different values of free magnetic energy, the magnetic energy of the NLFF magnetic configurations ($E_m^{\rm NLFF}$), and the relative magnetic helicity. We also mention the α-values used to compute the LFF fields satisfying Woltjer's theorem. We note that the different values of free energy are consistent and increase when the eruption phenomena increase in strength with the exception of $\Delta E_m^{\rm vir}$ from the observed magnetograms. The latter is related to the applicability of the virial theorem because the observed magnetograms are not force-free at the photospheric level (Metcalf et al. 1995).

5. CONCLUSIONS

We have computed the free magnetic energy from several formulae in various active regions at different stages of their

TABLE 1
FREE MAGNETIC ENERGY AND RELATIVE MAGNETIC HELICITY FOR THE DIFFERENT ACTIVE REGIONS

					$\Delta E_m^{\rm vir}$			
REGION	$E_m^{\rm NLFF}$ (10^{32} erg)	$\Delta E_{\rm pot}^{\rm NLFF}$ (10^{32} erg)	α ($\rm Mm^{-1}$)	$\Delta E_{\rm LFF}^{\rm NLFF}$ (10^{32} erg)	Observed (10^{32} erg)	Computed (10^{32} erg)	ΔH_m (10^{42} $\rm Mx^2$)	COMMENTS
AR 8151	0.64	0.26	0.067	0.05	1.2	0.79	0.47	Twisted bundles
AR 8210	10.6	0.24	−0.056	0.14	1.63	0.79	−4.2	Before C flare
AR 9077	14.2	2.21	−0.015	1.62	0.48	1.25	−14.6	Postflare loops
AR 10486	70.5	18.05	0.021	7.23	41.7	2.62	35.1	Before X17 flare

evolution: from the difference between the NLFF field and either the potential field ($\Delta E_{\rm pot}^{\rm NLFF}$) or the LFF field ($\Delta E_{\rm LFF}^{\rm NLFF}$) having the same magnetic helicity, and from the magnetic virial theorem ($\Delta E_m^{\rm vir}$) using either the observed field or the NLFF field.

The free magnetic energy $\Delta E_{\rm LFF}^{\rm NLFF}$ is a better estimate (than $\Delta E_{\rm pot}^{\rm NLFF}$) of the energy budget of an active region available for flaring assuming that the magnetic helicity is conserved and gives more insights into the possible eruption mechanisms in the active region. For AR 8151, it is clear that there is not enough energy to trigger a flare capable of a large-scale reorganization of the field ($\sim 5 \times 10^{30}$ erg). Therefore as stated in Régnier & Amari (2004) the kink instability of the highly twisted flux tube is most likely to be responsible for the observed eruptive phenomenon. Despite a magnetic energy of about 10^{33} erg, the free magnetic energy in AR 8210 is only 1% of the total energy but is enough to trigger small confined flares. This is consistent with the observations and modeling described in Régnier & Canfield (2006). We note that for the two possible mechanisms to store energy (Régnier & Priest 2007), the presence of large twisted flux bundles is more efficient than the highly complex topology: 10% of free energy in AR 8151 compared to 1% for AR 8210. The magnetic energy budget of AR 9077 is still important even if the observed field is after a X5.7 flare. Therefore even after a strong flare with postflare loops resembling potential field lines, the magnetic configuration is far from potential and the energy budget is still sufficient to trigger further powerful flares. For AR 10486, $\Delta E_{\rm LFF}^{\rm NLFF}$ is certainly not sufficient to trigger the observed X17.2 flare, but the $\Delta E_{\rm pot}^{\rm NLFF}$ seems to be more consistent with the recorded flaring activity. This can be explained by the fact that the main hypothesis of Woltjer's theorem is not satisfied: the X-class flare is associated with a CME expelling a magnetic cloud (and therefore magnetic helicity) into the interplanetary medium.

The free magnetic energy $\Delta E_m^{\rm vir}$ gives consistent values when computed from the NLFF extrapolated fields. For most photospheric magnetograms, the force-free assumption is not well satisfied and so leads to inaccurate values of $\Delta E_m^{\rm vir}$ from observations. In Metcalf et al. (2005) the computation of the free energy from the virial theorem was performed using chromospheric magnetic field measurements which are more force-free than photospheric magnetograms (Metcalf et al. 1995; Moon et al. 2002).

To have a better understanding of flaring activity, our main conclusion is that it is useful to compute both $\Delta E_{\rm pot}^{\rm NLFF}$ and $\Delta E_{\rm LFF}^{\rm NLFF}$: the first giving an upper limit on the magnetic energy that can be released during a large flare, especially when associated with a CME, the second being a good estimate of the energy budget for small flares and allowing us to distinguish between different flare scenarios.

We thank the UK STFC for financial support (STFC RG). The computations were done with XTRAPOL code developed by T. Amari (supported by the Ecole Polytechnique, Palaiseau, France and the CNES). We also acknowledge the financial support by the European Commission through the SOLAIRE network (MTRN-CT-2006-035484).

REFERENCES

Aly, J. J. 1984, ApJ, 283, 349
———. 1989, Sol. Phys., 120, 19
Amari, T., Aly, J. J., Luciani, J. F., Boulmezaoud, T. Z., & Mikic, Z. 1997, Sol. Phys., 174, 129
Amari, T., Boulmezaoud, T. Z., & Mikic, Z. 1999, A&A, 350, 1051
Amari, T., & Luciani, J.-F. 2000, Phys. Rev. Lett., 84, 1196
Berger, M. A. 1985, ApJS, 59, 433
Berger, M. A., & Field, G. B. 1984, J. Fluid Mech., 147, 133
Bleybel, A., Amari, T., van Driel–Gesztelyi, L., & Leka, K. D. 2002, A&A, 395, 685
Canfield, R. C., et al. 1993, ApJ, 411, 362
Fletcher, L., & Hudson, H. S. 2001, Sol. Phys., 204, 69
Grad, H., & Rubin, H. 1958, in Proc. 2nd Int. Conf. on Peaceful Uses of Atomic Energy, Vol. 31 (Geneva: United Nations), 190
Heyvaerts, J., & Priest, E. R. 1984, A&A, 137, 63
———. 1992, ApJ, 390, 297
Klimchuk, J. A., Canfield, R. C., & Rhoads, J. E. 1992, ApJ, 385, 327
Kusano, K., Maeshiro, T., Yokoyama, T., & Sakurai, T. 2002, ApJ, 577, 501
LaBonte, B. J., Mickey, D. L., & Leka, K. D. 1999, Sol. Phys., 189, 1
Liu, Y., & Zhang, H. 2001, A&A, 372, 1019
Mackay, D. H., & van Ballegooijen, A. A. 2006a, ApJ, 641, 577
Mackay, D. H., & van Ballegooijen, A. A. 2006b, ApJ, 642, 1193
Metcalf, T. R., Leka, K. D., & Mickey, D. L. 2005, ApJ, 623, L53
Metcalf, T. R., Mickey, D. L., McClymont, A. N., Canfield, R. C., & Uitenbroek, H. 1995, ApJ, 439, 474
Mickey, D. L., Canfield, R. C., LaBonte, B. J., Leka, K. D., Waterson, M. F., & Weber, H. M. 1996, Sol. Phys., 168, 229
Molodenskii, M. M. 1969, Soviet Astron.–AJ, 12, 585
Moon, Y.-J., Choe, G. S., Yun, H. S., Park, Y. D., & Mickey, D. L. 2002, ApJ, 568, 422
Nandy, D., Hahn, M., Canfield, R. C., & Longcope, D. W. 2003, ApJ, 597, L73
Régnier, S., & Amari, T. 2004, A&A, 425, 345
Régnier, S., Amari, T., & Canfield, R. C. 2005, A&A, 442, 345
Régnier, S., Amari, T., & Kersalé, E. 2002, A&A, 392, 1119
Régnier, S., & Canfield, R. C. 2006, A&A, 451, 319
Régnier, S., & Priest, E. R. 2007, A&A, 468, 701
Taylor, J. B. 1986, Rev. Mod. Phys., 58, 741
Wheatland, M. S., & Metcalf, T. R. 2006, ApJ, 636, 1151
Woltjer, L. 1958, Proc. Natl. Acad. Sci., 44, 489
Yan, Y., Deng, Y., Karlicky, M., Fu, Q., Wang, S., & Liu, Y. 2001, ApJ, 551, L115